J|A|C|S ARTICLES

Published on Web 05/22/2009

Circular Dichroism Spectrum of Peptides in the Poly(Pro)II Conformation

Robert W. Woody

Department of Biochemistry and Molecular Biology, Colorado State University, Fort Collins, Colorado 80523

Received February 16, 2009; E-mail: robert.woody@colostate.edu

Abstract: The poly(Pro)II (P_{II}) conformation is increasingly recognized as an important element in peptide and protein conformation. Circular dichroism (CD) is one of the most useful methods for detecting and characterizing P_{II}. Although the standard exciton-based model for predicting peptide CD spectra works well for α-helices and β-sheets, it fails to reproduce the P_{II} CD spectrum because it does not account for mixing of the $n\pi^*$ and $\pi\pi^*$ transitions with transitions in the deep UV, which is significant for the P_{II} conformation. In this work, the exciton model is extended to include this mixing, using ab initio-derived bond polarizability tensors to calculate the contributions of the high-energy transitions. The strong negative 195-nm and weaker positive 220-nm CD bands of P_{II} are reproduced for $(Ala)_n$ conformers in the P_{II} region of the Ramachandran map. For the canonical P_{II} conformation from fiber diffraction of poly(Pro)II (−77, +146), the results are poor, but conformations with less negative ϕ ($\sim -60°$) and more positive ψ ($\geq 160°$) give spectra showing the P_{II} characteristics. The CD of $(Pro)_n$ is not reproduced by the calculations, probably because variations in (ϕ,Ψ), ring puckering, and cis−trans isomerism are not included in the model The extended model also gives improved results for α-helical polypeptides, leading to increased amplitude for the 205-nm band and decreased amplitude for a negative band predicted near 180 nm.

Introduction

The left-handed 3-fold helix[1] adopted by poly(L-proline) in aqueous solution was initially considered to be limited to proline-rich polypeptides such as poly(Pro), poly(Hyp), and the $(Pro\text{-}X\text{-}Gly)_n$ polypeptides making up the collagen triple helix. The work of Tiffany and Krimm[2,3] showed that this conformation, called polyproline II (P_{II}), is an important component of nominally unordered polypeptides, such as poly(Lys) and poly(Glu) at neutral pH, i.e., in their charged forms. This conclusion, although not widely accepted at the time,[4] has received strong support from many subsequent studies.[5,6] P_{II} is now recognized not only as an important component of charged homopolypeptides, but of globular proteins,[7] unfolded proteins,[6] and of short oligopeptides.[8] Theoretical studies have shown that although P_{II} is not even at a local energy minimum on the dipeptide energy surface in vacuo, hydration stabilizes P_{II} markedly, making it the most stable conformer for some dipeptides in water.[9]

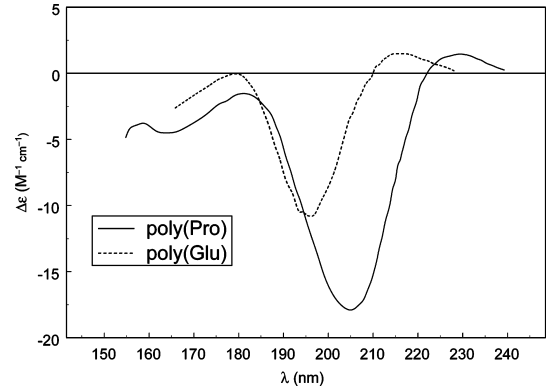

Figure 1. CD spectra of the poly(Pro) II (P_{II}) conformation. The spectrum of poly(Pro) in water[24] (—) is prototypical, with a strong negative band at 206 nm and a weak positive band at 225 nm. The spectrum of poly(Glu) in water[25] (– – –) is dominated by the P_{II} conformation,[2,5] as indicated by the CD spectrum, which resembles that of poly (Pro). The wavelength shift of ∼10 nm results from the difference between secondary and tertiary amides.

Most of Tiffany and Krimm's evidence was based on CD spectra, especially the remarkable similarity of the CD spectra of charged poly(Lys) and poly(Glu) to that of poly(Pro).[2] CD has continued to play a key role in the study of the P_{II} conformation.[5,6] Ironically, the CD spectra of poly(Pro) and of peptides in the P_{II} conformation (Figure 1) are poorly understood, and efforts to calculate the P_{II} spectrum by quantum mechanical methods, which have been successful for the α-helix and β-sheets, have been generally unsuccessful[4,5] in reproducing the P_{II} spectrum. The most successful calculation of the CD

(1) Cowan, P. M.; McGavin, S. *Nature* **1955**, *176*, 501–503.
(2) Tiffany, M. L.; Krimm, S. *Biopolymers* **1968**, *6*, 1379–1382.
(3) Krimm, S.; Tiffany, M. L. *Isr. J. Chem.* **1974**, *12*, 189–200.
(4) Woody, R. W. *J. Polym. Sci., Part D: Macromol. Rev.* **1977**, *12*, 181–320.
(5) Woody, R. W. *Adv. Biophys. Chem.* **1992**, *2*, 37–79.
(6) Shi, Z. S.; Woody, R. W.; Kallenbach, N. R. *Adv. Protein Chem.* **2002**, *62*, 163–240.
(7) Adzhubei, A. A.; Sternberg, M. J. E. *J. Mol. Biol.* **1993**, *229*, 472–493.
(8) Eker, F.; Cao, X. L.; Nafie, L.; Schweitzer-Stenner, R. *J. Am. Chem. Soc.* **2002**, *124*, 14330–14341.
(9) Han, W. G.; Jalkanen, K. J.; Elstner, M.; Suhai, S. *J. Phys. Chem. B* **1998**, *102*, 2587–2602.

10.1021/ja901218m CCC: $40.75

spectrum of poly(Pro) II is that of Applequist and co-workers,[10,11] who have used a dipole-interaction model[12] based upon the classical polarizability theory of DeVoe.[13] However, the DeVoe model only treats electronically allowed transitions, so the amide nπ^* transition is not included in Applequist's calculations.

It should be noted that, in contrast to the situation with simulations of electronic CD, successful simulations of vibrational CD (VCD) and Raman optical activity (ROA) have been reported for the P_{II} conformation.[14,15] Because these vibrational chiroptical spectroscopies utilize the electronic ground state, ab initio quantum mechanical calculations methods are more robust and can be applied to larger systems than is the case for electronically excited states. Further, vibrational modes are more localized than the electronic exciton modes, so high-level calculations can be performed for smaller systems to provide parameters that are transferable to larger systems. Experimentally, however, electronic CD instrumentation is much more widely available than ROA and VCD instrumentation, so it is imperative to resolve the more difficult problem of understanding the electronic CD spectrum of the P_{II} conformation.

Calculations based upon the quantum mechanical exciton model[16−21] have in some cases reproduced the negative CD band near 200 nm that is characteristic of the P_{II} spectrum (Figure 1). However, the exciton model by itself is inherently incapable of accounting for another salient feature of the spectrum: the CD is negative throughout the 190-nm $\pi\pi^*$ band. Mixing of only the nπ^* and the 190-nm $\pi\pi^*$ band will always lead to equal areas of positive and negative CD at wavelengths of 175 nm and above. A CD spectrum that exhibits positive and negative bands of equal area is said to be *conservative*. The P_{II} spectrum is distinctly nonconservative at wavelengths above 175 nm. The strongly nonconservative character of the P_{II} CD spectrum must reflect mixing of the nπ^* and $\pi\pi^*$ transitions with transitions at higher energy. Ronish and Krimm[19] took such transitions into account by using a polarizability approximation. Indeed, their predicted spectrum reproduced the P_{II} spectrum quite well. However, this agreement was achieved by arbitrarily assigning a larger bandwidth to the exciton components (14 nm) and a smaller bandwidth to the polarizability contributions (10 nm), thus diminishing the positive contributions from the excitons. Moreover, the bond and group polarizabilities, and especially the anisotropies, that they used are suspect because they were based[22] on Kerr effect studies[23] and were subject to large uncertainties.

It is therefore clear that a successful calculation of P_{II} CD by a quantum mechanical model must incorporate mixing of the nπ^* and $\pi\pi^*$ transitions with high-energy transitions, which can be accomplished via the polarizability approximation.[26] The problem here has been that polarizability tensors are needed, i.e., anisotropic polarizabilities, rather than the mean (scalar) polarizabilities. Most previous quantum mechanical applications of the polarizability approximation have used the polarizability anisotropies proposed by Woody and Tinoco,[22] which are suspect, as noted previously. Fortunately, ab initio methods can now provide reliable polarizabilities. Using localized orbitals, Garmer and Stevens[27] have calculated polarizability tensor components for individual bonds and lone pairs that are ideally suited for the present application and are used in the present work.

Most previous applications of the polarizability approximation have also been limited by two other approximations. In nearly all cases, the point-dipole approximation has been used for the interaction of the transition charge densities with the polarizable groups, rather than the more accurate monopole approximation for the transition charge density. Except for a few studies,[28−30] previous workers have neglected the exciton splitting in calculating the mixing with the $\pi\pi^*$ transition. This yields the net contribution to the rotational strength from the polarizable groups, but in summing over the exciton levels, significant contributions of opposite sign in different regions of the exciton band may be lost. Both of these approximations are avoided in the present work.

This work also includes two additional refinements. (1) The mixing of the exciton transitions with transitions to doubly excited configurations is treated, using first-order perturbation theory. As has been generally assumed, the contribution of this effect is small and its neglect in previous studies is largely justified. (2) The polarizability approximation is used to calculate the shifts in wavelength of the exciton components (a few nanometers) and changes in dipole strength. These effects are significant. The wavelength shifts acting differentially on the exciton levels reverse the sign of the exciton couplet for some P_{II} conformations. The changes in dipole strength are largely responsible for hypo- and hyperchromism in these polypeptides.

The focus of this paper is on the P_{II} conformation of polypeptides with secondary amides modeled by oligo- and poly(Ala) for which the exciton model, extended to include polarizable group contributions, provides a good description of the CD spectrum. The model also works well for some reported collagen structures. Available structures of poly(Pro) itself give poor results. It is proposed that the CD of poly(Pro) in solution is affected significantly by variations in the Ramachandran angles ϕ and Ψ, ring puckering, and cis−trans isomerism.

Methods

Geometries for oligo(Ala) peptides were generated from standard peptide geometry, using standard methods.[31,32] Tetrahedral bond

(10) Applequist, J. *Biopolymers* **1981**, *20*, 2311–2322.
(11) Bode, K. A.; Applequist, J. *J. Phys. Chem.* **1996**, *100*, 17825–17834.
(12) Applequist, J.; Sundberg, K. R.; Olson, M. L.; Weiss, L. C. *J. Chem. Phys.* **1979**, *70*, 1240–1246.
(13) Devoe, H. *J. Chem. Phys.* **1965**, *43*, 3199–3208.
(14) Zhu, F.; Kapitan, J.; Tranter, G. E.; Pudney, P. D. A.; Isaacs, N. W.; Hecht, L.; Barron, L. D. *Proteins-Struct. Funct. Bioinform.* **2008**, *70*, 823–833.
(15) Bour, P.; Kubelka, J.; Keiderling, T. A. *Biopolymers* **2002**, *65*, 45–59.
(16) Pysh, E. S. *J. Mol. Biol.* **1967**, *23*, 587–599.
(17) Madison, V.; Schellman, J. *Biopolymers* **1972**, *11*, 1041–1076.
(18) Tterlikkis, L.; Loxsom, F. M.; Rhodes, W. *Biopolymers* **1973**, *12*, 675–684.
(19) Ronish, E. W.; Krimm, S. *Biopolymers* **1974**, *13*, 1635–1651.
(20) Pysh, E. S. *Biopolymers* **1974**, *13*, 1563–1571.
(21) Manning, M. C.; Woody, R. W. *Biopolymers* **1991**, *31*, 569–586.
(22) Woody, R. W.; Tinoco, I., Jr. *J. Chem. Phys.* **1967**, *46*, 4927–4945.
(23) LeFevre, C. G.; LeFevre, R. J. W. *Rev. Pure Appl. Chem.* **1955**, *5*, 261–318.
(24) Jenness, D. D.; Sprecher, C.; Johnson, W. C. *Biopolymers* **1976**, *15*, 513–521.
(25) Johnson, W. C., Jr.; Tinoco, I., Jr. *J. Am. Chem. Soc.* **1972**, *94*, 4389–4390.
(26) Tinoco, I., Jr. *Adv. Chem. Phys.* **1962**, *4*, 113–160.
(27) Garmer, D. R.; Stevens, W. J. *J. Phys. Chem.* **1989**, *93*, 8263–8270.
(28) Zubkov, V. A.; Vol'kenshtein, M. V. *Mol. Biol.* **1970**, *4*, 483–490.
(29) Johnson, W. C., Jr.; Itzkowitz, M.; Tinoco, I., Jr. *Biopolymers* **1972**, *11*, 225–234.
(30) Rabenold, D. A.; Rhodes, W. *J. Phys. Chem.* **1986**, *90*, 2560–2566.
(31) Ooi, T.; Scott, R. A.; Vanderkooi, G.; Scheraga, H. A. *J. Chem. Phys.* **1967**, *46*, 4410–4426.

angles were assumed at the α-carbon. To cover the P_{II} region, the Ramachandran angle ϕ was varied from −60° to − 80° and Ψ from +140° to +185°, in 5° intervals.

The exciton calculations included the peptide nπ^*, NV_1 (190-nm $\pi\pi^*$), and NV_2 (140-nm $\pi\pi^*$) transitions. The nπ^* transition was located at 220 nm, and its magnetic dipole transition moment and transition charge density were calculated from ZINDO/S[33] wave functions, as previously described,[34] with minor modifications.[35] The NV_1 transition was placed at 190 nm for secondary amides and at 200 nm for tertiary amides (X-Pro bonds). The magnitude of the NV_1 electric dipole transition moment was taken to be 3.02 D,[36] but the direction was allowed to vary from −55° to −40°, the approximate directions reported for secondary and primary amides, respectively.[36,37] (By Clark's convention,[36] amide transition moment directions are specified relative to the C═O bond direction, with the C−N direction positive.) The NV_2 transition dipole moment was fixed in magnitude (1.72 D), and the direction was one of the two possible values reported by Clark[36] (+61°). No mixing between the NV_1 and NV_2 transitions within a peptide was allowed, but nπ^*-NV_1 and nπ^*-NV_2 mixing were considered, using previously described parameters.[34,35]

The standard exciton model[38−40] for polypeptides, the basis of the matrix method,[41] starts with the Hamiltonian for the polypeptide:

$$H = \sum_i H_i + \sum_i \sum_{j>i} V_{ij} \tag{1}$$

where H_i is the Hamiltonian for group i and V_{ij} is the Coulombic interaction of the electrons and nuclei in group i with those in group j. This Hamiltonian is based upon the assumption that the molecule can be divided into distinct groups between which electron exchange is negligible. If exchange among the groups is negligible, the ground state of the polypeptide can be taken to be the product of the ground-state wave functions of the individual groups, ϕ_{i0}, each of which is the lowest energy solution of the Schrödinger equation for the group i

$$H_i\phi_i = E_i\phi_i \tag{2}$$

Thus,

$$\Psi_0 = \prod_{i=1}^{N} \phi_{i0} \tag{3}$$

In the usual exciton model, excited configurations of the polypeptide are constructed by exciting a single group to one of its excited states a, b, c,... Excited states of the polypeptide are constructed by taking linear combinations of these excited configurations:

$$\Psi_K = \sum_i \sum_a C_{iaK}\psi_{ia} \tag{4}$$

where ψ_{ia} is a singly excited configuration in which group i is excited to state a and all other groups are in their ground state:

$$\psi_{ia} = \phi_{10}\phi_{20} \ldots \phi_{ia} \ldots \phi_{NO} \tag{5}$$

The C_{iaK} are the coefficients that characterize the contribution of excited configuration ia to exciton state K. In the matrix method,[41] the matrix form of the Hamiltonian of eq 1 is diagonalized, yielding the exciton frequencies, E_K, as the eigenvalues, and the exciton coefficients, C_{iaK}, as the eigenvectors.

In the usual matrix method as applied to polypeptides, two or three low-lying excited states of the peptide are considered. Moreover, only singly excited configurations are treated. Thus, the usual matrix method omits higher excited states of the monomers. In this paper, the matrix method is extended to include these higher excited states.

First-order perturbation theory[26] gives the following expression (see the Supporting Information), for the rotational strength of exciton level K resulting from the mixing of the high-energy states with the electrically allowed transitions (discrete excited states—nπ^*, NV_1, NV_2—are denoted by lower case Roman letters and high-energy excited states by lower case Greek letters):

$$(R_\mu)_{KK} = -\frac{2\pi}{\lambda_k}\sum_{ia}^{N}\sum_{ja}^{N}\sum_{l\neq i,j}^{N}\sum_{\beta} C_{iaK}C_{jbK}\frac{\nu_\beta V_{job;lo\beta}}{h(\nu_\beta^2 - \nu_K^2)}\mathbf{R}_{il}\cdot\boldsymbol{\mu}_{lo\beta}\times\boldsymbol{\mu}_{ioa} \tag{6}$$

where ν_β and $\boldsymbol{\mu}_{lo\beta}$ are, respectively, the frequency and the electric dipole transition moment of the high-energy transition; ν_K and λ_K are the exciton frequency (in Hz) and wavelength; $\boldsymbol{\mu}_{ioa}$ is the electric dipole transition moment of $0\rightarrow a$ in group i; $\mathbf{R}_{il} = (\mathbf{R}_l - \mathbf{R}_i)$ is the vector from the group i to group l; and $V_{job;lo\beta}$ is the energy of interaction between discrete transition $0\rightarrow b$ in group j and high-energy transition $0\rightarrow\beta$ in group l. The expression is equivalent to eq IIIB-22f of Tinoco,[26] but Tinoco summed over exciton states. Zubkov and Vol'kenshtein[42] also derived this expression (their eq 2).

In the monopole approximation, the transition charge density described by $\boldsymbol{\mu}_{\mathrm{job}}$ is represented by a set of point charges, q_{jbt}, positioned at points $\boldsymbol{r}_{jbt}$, such that

$$\sum_t q_{\mathrm{jbt}}\mathbf{r}_{\mathrm{jbt}} = \boldsymbol{\mu}_{job} \tag{7}$$

The interaction energy between the transition charge densities of $0\rightarrow b$ in group j and $0\rightarrow\beta$ in group l is given by

(32) McGuire, R. F.; Vanderkooi, G.; Momany, F. A.; Ingwall, R. T.; Crippen, G. M.; Lotan, N.; Tuttle, R. W.; Kashuba, K. L.; Scheraga, H. A. *Macromolecules* **1971**, *4*, 112–124.
(33) Ridley, J.; Zerner, M. *Theor. Chim. Acta* **1973**, *32*, 111–134.
(34) Woody, R. W.; Sreerama, N. *J. Chem. Phys.* **1999**, *111*, 2844–2845.
(35) Errors in calculating some of the transition monopoles and transition moments in ref 34 were discovered. The nπ^* and NV_1 monopoles and the NV_2 transition gradient are opposite in sign to those reported in ref 34. In addition, the transition monopole charges connecting the nπ^* and NV_2 states included charges on the carbonyl carbon rather than the amide nitrogen. The corrected transition parameters are listed in Tables S5−S8 of the Supporting Information. The effects of these changes are not large because the matrix elements governing the nπ^*−nπ^*, NV_1−NV_1, NV_2−NV_2, and nπ^*−NV_1 mixing via coupled oscillator interactions are all unchanged. The corresponding $\nabla_i\cdot(\mathbf{r}_j\times\nabla_j)$ and $\nabla_i\cdot\mathbf{m}_j$ factors are also unchanged. Those matrix elements governing the nπ^*−NV_2 and NV_1−NV_2 mixing through coupled-oscillator interactions are reversed in sign, but so are the corresponding $\nabla_i\cdot\mathbf{m}_j$ and $\nabla_i\cdot(\mathbf{r}_j\times\nabla_j)$ factors, so the resulting rotational strengths are, to first order, unaffected. Of the one-electron terms, those from nπ^* and NV_1 mixing are also unaffected because both the V matrix elements and the $\nabla_i\cdot\mathbf{m}_j$ factors are reversed in sign. Only in the case of the nπ^*−NV_2 one-electron mixing do the above sign changes lead to a reversal in sign of the rotational strength contributions. A comparison of the calculated CD spectrum of a 20-amide Pauling and Corey α-helix using the corrected and uncorrected transition parameters is given in Figure S1 of the Supporting Information. The corrections lead to a ∼30% increase in the magnitude of the nπ^* band, a ∼25% increase in the 208-nm band, and less than a 2% increase in the 190-nm positive band.
(36) Clark, L. B. *J. Am. Chem. Soc.* **1995**, *117*, 7974–7986.
(37) Peterson, D. L.; Simpson, W. T. *J. Am. Chem. Soc.* **1957**, *79*, 2375–2382.
(38) Moffitt, W. *J. Chem. Phys.* **1956**, *25*, 467–478.
(39) Davydov, A. S. *Theory of Molecular Excitons*; Plenum Press: New York, 1971.
(40) Harada, N.; Nakanishi, K. *Circular Dichroic Spectroscopy: Exciton Coupling in Organic Stereochemistry*; University Science Books: Mill Valley, CA, 1983.
(41) Bayley, P. M.; Nielsen, E. B.; Schellman, J. A. *J. Phys. Chem.* **1969**, *73*, 228–243.
(42) Zubkov, V. A.; Birshtein, T. M.; Milevskaya, I. S.; Vol'kenshtein, V. M. *Biopolymers* **1971**, *10*, 2051–2061.

$$V_{job;lo\beta} = -\sum_t \frac{q_{jbt}\mathbf{R}_{jbt,lo\beta}\cdot\boldsymbol{\mu}_{lo\beta}}{|\mathbf{R}_{jbt,lo\beta}|^3} \quad (8)$$

where $\mathbf{R}_{jbt,lo\beta} = (\mathbf{R}_{lo\beta} - \mathbf{R}_{jbt})$ is the vector from the monopole *jbt* to group *l*. Substituting this into the expression for $(R_\mu)_{KK}$, we obtain

$$(R_\mu)_{KK} = -\frac{2\pi}{\lambda_k}\sum_{ia}\sum_{jb}\sum_t\sum_{l\neq j}\sum_\beta C_{iaK}C_{jbK}\times \frac{\nu_\beta q_{jbt}\mathbf{R}_{jbt,lo\beta}\cdot\boldsymbol{\mu}_{lo\beta}\boldsymbol{\mu}_{lo\beta}\cdot\boldsymbol{\mu}_{ioa}\times\mathbf{R}_{il}}{h(\nu_\beta^2 - \nu_K^2)|\mathbf{R}_{jbt,lo\beta}|^3} \quad (9)$$

The sum over high-energy transitions of $\nu_\beta\boldsymbol{\mu}_{lo\beta}\boldsymbol{\mu}_{lo\beta}$ can be replaced by a polarizability tensor and an average frequency $\nu_0 \approx 10^5$ cm^{-1} to give

$$(R_\mu)_{KK} = \frac{\pi\nu_0^2}{\lambda_K(\nu_0^2 - \nu_K^2)}\sum_{ia}\sum_{jb}\sum_{l\neq j}\sum_t C_{iaK}C_{jbK}\frac{q_{jbt}\mathbf{R}_{jbt,lo\beta}\cdot\boldsymbol{\alpha}_l\cdot\boldsymbol{\mu}_{ioa}\times\mathbf{R}_{il}}{|\mathbf{R}_{jbt,lo\beta}|^3} \quad (10)$$

This multiple summation can be conveniently formulated as a matrix multiplication:

$$\mathbf{R}_\mu = \gamma_\mu\sum_l \mathbf{C}^+\mathbf{G}\boldsymbol{\alpha}_l\mathbf{F}\mathbf{C} \quad (11)$$

where $\gamma_\mu = \pi\nu_0^2/[\lambda_K(\nu_0^2 - \nu_K^2)]$; **C** is a matrix with eigenvectors as columns; $\mathbf{C}^+$ is the transpose of **C**, with eigenvectors as rows; **G** is a matrix with the general element

$$G_{jl} = \sum_t \frac{q_{jt}\mathbf{R}_{jbt,l}}{|\mathbf{R}_{jbt,l}|^3} \quad (12)$$

and $\boldsymbol{\alpha}_l$, the polarizability matrix of group ***l***, has 3 × 3 submatrices along the diagonal. These are the polarizability tensors for the peptide groups. Off-diagonal submatrices are zero. **F** is a matrix with the general element:

$$\mathbf{F}_{ial} = \boldsymbol{\mu}_{ioa}\times\mathbf{R}_{il} \quad (13)$$

where $\mathbf{R}_{il} = \mathbf{R}_l - \mathbf{R}_i$ is the vector from the center of transition *i* to the polarizable group *l*. The matrix product $\mathbf{R}_\mu$ is a square matrix with dimensions $3N_p \times 3N_p$. The diagonal element $(R_\mu)_{KK}$ is the contribution of the polarizable groups to the rotational strength of exciton level *K* through mixing with the electric dipole transition moments of the discrete transitions.

The contributions to the rotational strength of exciton level *K* from magnetically allowed transitions mixing with the high-energy transitions are given by first-order perturbation theory[26] (see Supporting Information) as

$$(R_m)_{KK} = -2\sum_{ia}^N\sum_{jb}^N\sum_{l\neq i,j}^N\sum_\beta C_{iaK}C_{jbK}\frac{V_{ioa;lo\beta}}{h(\nu_\beta^2 - \nu_K^2)}\mathrm{Im}[\boldsymbol{\mu}_{lo\beta}\cdot\mathbf{m}_{jb0}^*] \quad (14)$$

where $\mathbf{m}_{jb0}^*$ is the complex conjugate of the magnetic dipole transition moment of transition $0\rightarrow b$ in group *j*. Making the monopole approximation and using the sum over high-energy transitions as before, we obtain the matrix equation:

$$R_m = \gamma_m\mathrm{Im}\sum_l \mathbf{C}^+\mathbf{G}\boldsymbol{\alpha}_l\mathbf{m}^+\mathbf{C} \quad (15)$$

where the diagonal elements of the matrix $\mathbf{R}_m$, $(R_m)_{KK}$, are the contributions of the polarizable groups to the *K*th exciton rotational strength through mixing with magnetically allowed discrete transitions; $\gamma_m = \nu_0^2/(\nu_0^2 - \nu_K^2)$; and $\mathbf{m}^+$ is a $3N_\alpha \times 3N_p$ matrix, the *i*th column of which consists of N_α repetitions of the components of $\mathbf{m}_i^*$.

We also consider the mixing of doubly excited configurations with the ground and singly excited configurations. To first order, mixing of singly and doubly excited configurations does not contribute to the electric and magnetic dipole transition moments. Mixing of doubly excited configurations with the ground configuration does contribute to the transition moments and in first order, giving

$$(\Psi_0|\nabla|\Psi_{AK}) = \sum_{i,a} C_{iaK}\left\{\nabla_{ioa} + \sum_{k,c}\frac{V_{i0a;k0c}}{h(\nu_a + \nu_c)}\nabla_{koc}\right\} \quad (16)$$

and

$$(\Psi_0|\mathbf{rx}\nabla|\Psi_{AK}) = \sum_{j,b} C_{jbK}\left\{(\mathbf{rx}\nabla)_{job} + \sum_{l,d}\frac{V_{j0b;l0d}}{h(\nu_b + \nu_d)}(\mathbf{r}\times\nabla)_{lod}\right\} \quad (17)$$

The rotational strength R_{0K} is obtained from the scalar product:

$$R_{OK} = (\gamma_P/E_K)\mathrm{Im}\{\nabla_{0K}\cdot(\mathbf{rx}\nabla)_{0K}\} = R_{OK}^{(0)} + R_{OK}^{(1)} \quad (18)$$

where $\gamma_P = e^2\hbar^3/2m^2c$ and E_K is the energy of exciton transition *K*. (It will be noted that we are using the dipole velocity form of the rotational strength here, as we do in the exciton calculation. This formulation guarantees that the rotational strength will be independent of origin.[38] By contrast, in calculating the polarizable group contributions, we have used the dipole length form. This is permissible in this case because all terms involving position vectors appear as differences in position, as in eqs 6 and 8−13, and are therefore origin-independent.) The zeroth order term, $R_{0K}^{(0)}$, is the usual exciton rotational strength. We are interested here in the first-order terms, derived in the Supporting Information:

$$R_{0K}^{(1)} = (\gamma_P/E^K)\sum_{i,a}\sum_{j,b} C_{iaK}C_{jbK}\left\{\sum_{k,c}\frac{V_{i0a;k0c}}{h(\nu_a + \nu_c)}\nabla_{k0c}\cdot(\mathbf{r}\times\nabla)_{j0b} + \sum_{l,d}\frac{V_{j0b;l0d}}{h(\nu_b + \nu_d)}\nabla_{i0a}\cdot(\mathbf{r}\times\nabla)_{l0d}\right\} \quad (19)$$

First-order perturbation theory (see Supporting Information) gives the following matrix product for the shift in energy of exciton level *K* caused by mixing with the high-energy transitions in group *l*:

$$\Delta E_K = -\gamma_E\sum_l \mathbf{C}^+\mathbf{G}\boldsymbol{\alpha}_l\mathbf{G}^+\mathbf{C} \quad (20)$$

where $\gamma_E = \nu_0/[2(\nu_0 - \nu_K)]$ and the other matrices are as previously defined. The change in dipole strength of exciton level *K*, ΔD_K, produced by mixing with the high-energy transitions in group *l* is given by

$$\Delta D_K = -\gamma_D\sum_l \mathbf{C}^+\boldsymbol{\mu}\boldsymbol{\alpha}_l\mathbf{G}^+\mathbf{C} \quad (21)$$

where $\gamma_D = 2\nu_0^2/(\nu_0^2 - \nu_K^2)$ and $\boldsymbol{\mu}$ is a $3N_p \times 3N_\alpha$ matrix in which row *j* consists of N_α repetitions of the three components of $\boldsymbol{\mu}_{job}$. This equation is derived in the Supporting Information.

We considered 11 polarizable groups per Ala residue, all but one corresponding to a bond or a lone pair, and 18 groups for a Pro residue (Table 1). The polarizability tensors for the backbone groups were rendered axially symmetric by the following procedure.

Table 1. Polarizability Parameters[a]

group	$\alpha_{\parallel}-\alpha_{\perp}$[b]	$\alpha_{\perp}$[b]	symmetry axis
C′═O	5.40	3.91	∼C′═O bond
O lone pair 1	1.21	1.39	∼⊥C_α−C′ bond
O lone pair 2	2.01	0.98	∼∥C_α−C′ bond
C_α−C′	3.85	1.91	∼∥C_α−C′ bond
C′−N	5.56	5.43	∼C′−N bond
N−H	−2.90	2.68	⊥ amide plane
N−C_α	4.02	0.76	∼N−C_α bond
$\pi\pi^*$ trans[c]	−1.66	−0.16	∼C′═O bond
C_α−H	2.74	2.90	C_α−H bond
C_α−C_β	3.54	2.49	C_α−C_β bond
C_β methyl	8.22	8.70	3-fold axis

[a] On the basis of bond and lone-pair polarizability tensors calculated for *trans-N*-methylacetamide by Walter Stevens using the method of Garmer and Stevens.[27] For the C_α−C_β, C_α−H, and C_β methyl groups, the generic polarizability tensors given in Table 4 of the Garmer and Stevens paper are used. The positioning of the polarizabilities and details of the symmetry axes are described in the Supporting Information. [b] Units of polarizability: $a_0^3 = 0.148$ Å^3. [c] The "group" labeled '$\pi\pi^*$ trans' corresponds to the polarizability contributions of the 190- and 140-nm $\pi\pi^*$ transitions. These are subtracted (hence the minus signs) because they are treated explicitly in the exciton calculations.

Except for the banana bonds representing the carbonyl bond, the *xz*, *yz*, *zx*, and *zy* tensor elements were very small, $\sim 10^4$-fold smaller than the diagonal elements. In the case of the banana bonds, these elements were significant, but they were of opposite sign and of nearly equal magnitude for the two banana bonds representing the carbonyl bond. Therefore, when the banana bonds were combined, the resultants were comparable to those for the other polarizable groups. Thus, the *xz*, *yz*, *zx*, and *zy* tensor elements were set to zero for all polarizable groups. The submatrix for the in-plane components,

$$\begin{pmatrix} \alpha_{xx} & \alpha_{xy} \\ \alpha_{yx} & \alpha_{yy} \end{pmatrix} \tag{22}$$

was then diagonalized. The resulting diagonal submatrix was then substituted for the original submatrix in the polarizability matrix, giving rise to the diagonal 3 × 3 matrix:

$$\begin{pmatrix} \alpha_{x'x'} & 0 & 0 \\ 0 & \alpha_{y'y'} & 0 \\ 0 & 0 & \alpha_{zz} \end{pmatrix} \tag{23}$$

where $\alpha_{x'x'}$ and $\alpha_{y'y'}$ are the principal components in the $x'y'$ plane after rotation of the *x* and *y* axes, and α_{zz} is the *z* component of the polarizability. Generally, two of the diagonal elements were similar in magnitude. The two most similar values were averaged and the direction of the third component was taken to be the symmetry axis.

One polarizable group is centered at the carbonyl carbon and has a negative polarizability corresponding to the contributions of the NV_1 and NV_2 transitions. This avoids double-counting these contributions, which are included in the exciton calculations. The static polarizability resulting from the discrete transitions is, in dyadic form:

$$\alpha = (2/h)\sum_i \mu_i\mu_i/\nu_i \tag{24}$$

where the summation is over the two $\pi\pi^*$ transitions. The corresponding tensor form was diagonalized and approximated by an axially symmetric tensor as described above. The negative of this polarizability tensor was then used in the calculations.

The side-chain groups of Pro contain C−C and C−H bonds that are axially symmetric. They were treated using the mean polarizability parameters given in Table 4 of Garmer and Stevens.[27] The methyl group of Ala was treated as single group with its symmetry axis along the 3-fold axis, and was located on this axis at the point defined by the projection of the midpoints of the three C−H bonds (0.18 Å from the carbon).

The principal values and the symmetry axes of the polarizability ellipsoids are specified in Table 1, with further details given in the Supporting Information.

The polarizability tensor for an axially symmetric group in an arbitrary coordinate system can be expressed conveniently in dyadic form as

$$\alpha = (\alpha_{33} - \alpha_{11})\mathbf{e}_3\mathbf{e}_3 + \alpha_{11}\mathbf{1} \tag{25}$$

where $\mathbf{e}_3$ is the unit vector in the direction of the symmetry axis; α_{33} and α_{11} are, respectively, the polarizabilities parallel and perpendicular to the symmetry axis; and **1** is the unit dyadic.

CD spectra were calculated from the theoretical wavelengths of the exciton bands, λ_K, and the rotational strengths, R_K, assuming Gaussian band shapes:

$$\Delta\varepsilon = \sum_K \Delta\varepsilon_K^0 \exp\{-(\lambda - \lambda_K)^2/\Delta_K^2\} \tag{26}$$

where $\Delta\varepsilon_K^0$ is the amplitude of the *K*th exciton band and Δ_K is the half-bandwidth at 1/*e* of the maximum. The amplitude of the *K*th exciton band is related to the rotational strength and the bandwidth:[43]

$$\Delta\varepsilon_K^0 = 2.278R_K\lambda_K/\Delta_K \tag{27}$$

The half-bandwidth is calculated as a weighted average of the half-bandwidths for the monomer transitions, Δ_{ia}:

$$\Delta_K = \sum_i \sum_a C_{iaK}^2\Delta_{ia} \tag{28}$$

where C_{iaK} is the exciton coefficient defined in eq 4. The Δ_{ia} were taken to be[34] 10.5, 11.3, and 7.2 nm, respectively, for the nπ^*, NV_1, and NV_2 transitions.

Results

We first consider poly(Ala) in the canonical P_{II} conformation [(ϕ, Ψ) = (−78, +147)]. Calculations of the CD spectrum of a canonical 20-residue[44] P_{II} helix, including the exciton and polarizable group contributions, were performed using the NV_1 transition moment direction $\theta = -55°$.[36] This direction was determined by Clark[36] for crystals of a model secondary amide, N-acetylglycine. A study of the CD of the α-helix[45] showed that this transition moment direction gave significantly better results in exciton calculations than the older value of ∼ −40° based on single-crystal studies of primary amides.[36,37]

The results for a 20-amide P_{II} helix in the canonical conformation are shown in Figure 2. The exciton contribution calculated by the standard exciton model (green curve in Figure 2) shows a modest positive couplet centered near 212 nm, which results from a positive nπ^* band and a negative band from the parallel-polarized $\pi\pi^*$ exciton component.[38] A strong positive

(43) Moscowitz, A. Theory and analysis of rotatory dispersion curves. In *Optical Rotatory Dispersion: Applications to Organic Chemistry*; Djerassi, C., Ed.; McGraw-Hill: New York, 1960; pp 150−177.
(44) The calculations were actually performed for a P_{II} helix with 20 *amides*, not 20 *residues*. An unblocked peptide with *n* residues has *n*−1 amides. N-Acetylation or N-methylamidation at the C-terminus gives *n* amides, and blocking both termini gives *n* + 1 amides. Thus, N-Ac$(Ala)_{20}$ or $(Ala)_{20}$NMe would be a more accurate description of the system used here, but for simplicity we shall denote a helix with *n* amides by $(Ala)_n$, $(Pro)_n$, etc.
(45) Chin, D. H.; Woody, R. W.; Rohl, C. A.; Baldwin, R. L. *Proc. Natl. Acad. Sci. U.S.A.* **2002**, *99*, 15416–15421.

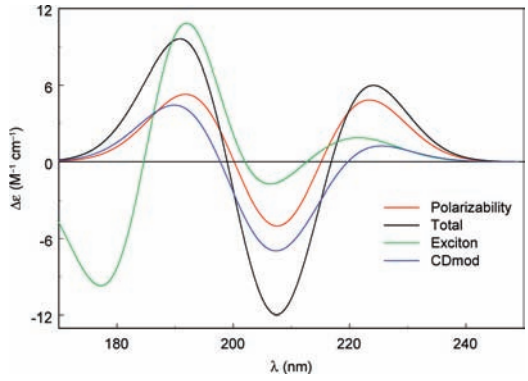

Figure 2. Calculated CD spectrum of $(Ala)_{20}$ with $(\phi, \Psi) = (-78, 147)$, the canonical P_{II} conformation. The transition moment of the 190-nm $\pi\pi^*$ transition was taken to be at $-55°$ relative to the amide C═O bond. The total CD spectrum is shown in black. The exciton spectrum calculated with exciton wavelengths is shown in green, the exciton spectrum calculated with wavelengths shifted by mixing with high-energy transitions is shown in blue, and the polarizability contribution is in red.

couplet is centered near 184 nm, resulting from the splitting of the perpendicularly polarized exciton components which, in the limit of the infinite helix, gives the helix band.[46−48]

The blue curve in Figure 2 shows the CD spectrum calculated using the exciton rotational strengths with the frequencies shifted by coupling with polarizable groups (eq 20). This spectrum differs strikingly from the exciton spectrum calculated using the exciton frequencies (green). In particular, the positive couplet at 184 nm in the unshifted spectrum is replaced by a weaker negative couplet centered at 199 nm in the shifted spectrum. The short-wavelength negative components from the exciton calculations are red-shifted more strongly than the long-wavelength positive exciton components, leading to a reversal in sign of the short-wavelength couplet. The negative long-wavelength parallel exciton band at 206 nm in the unshifted spectrum (green) disappears because it merges with the negative lobe of the helix band.

The polarizability contribution to the CD spectrum (red) is qualitatively like that of the frequency-shifted exciton spectrum, with a positive long-wavelength band and a negative couplet at shorter wavelengths. However, in contrast to the exciton spectrum, the polarizability contribution is nonconservative, with a significant excess of positive CD intensity. It should be noted that the polarizability contribution is comparable in magnitude to the exciton contribution. Moreover, it varies in sign across the NV_1 region, demonstrating that it is important to consider the contribution to each exciton state. Summing over the exciton levels, as has been done in most previous calculations, leads to extensive cancellation and underestimation of the polarizable group contribution.

The total CD (black) is the sum of the frequency-shifted exciton and polarizability contributions (blue and red, respectively). The $n\pi^*$ region has a substantial positive band and the $\pi\pi^*$ region is characterized by a strong negative couplet. The resulting spectrum is distinctly different from the experimental P_{II} spectrum (Figure 1), which shows a relatively weak positive $n\pi^*$ band and, most significantly, negative CD throughout the $\pi\pi^*$ region. In addition, the calculated spectrum is modestly nonconservative but exhibits a bias toward positive CD, not negative as experimentally observed. Thus, even with high-energy transitions taken into account, theory and experiment differ strongly for the standard P_{II} conformation. This is in agreement with the results of most previous exciton calculations.[16−18,21,49,50]

Prior studies[17−19,21] have found that alternative conformations in the P_{II} region of the Ramachandran map give results that are in better agreement with experiment than those from the canonical P_{II} conformation. Therefore, we have examined the P_{II} region using (ϕ, Ψ) pairs at 5° intervals, with ϕ ranging from $-80°$ to $-60°$ and Ψ from 140° to 185°. However, for $\theta_{NV1} = -55°$, the pattern found for the canonical P_{II} conformation is remarkably robust. Over the whole range, a strong positive couplet is obtained in the exciton calculations, which becomes a strong negative couplet upon inclusion of polarizability contributions. The only qualitative variation is found in the $n\pi^*$ region, with strong positive bands predicted for smaller Ψ values, diminishing with increasing Ψ. Near the upper limit of the range of Ψ, the CD at long wavelengths is negative, but there is no negative maximum near 220. The negative CD at 220 nm and above is part of the negative lobe of the $\pi\pi^*$ couplet, the maximum of which shifts to ~215 nm for $\Psi \sim 185°$. In all cases, the exciton CD calculated with exciton frequencies gives a positive couplet that is converted to a negative couplet when polarizability-induced frequency shifts are taken into account.

Because no conformation in the P_{II} region gave satisfactory results for $\theta = -55°$, we have used $\theta = -40°$, a value comparable to the NV_1 transition moment direction in primary amides[36,37] and used in nearly all previous calculations of polypeptide CD. A survey of the P_{II} region showed that for $\theta = -40°$, $(Ala)_{20}$ is predicted to have a CD spectrum qualitatively consistent with experiment for $\phi = -60°$ or $-65°$ and $\Psi \geq +160°$; for $\phi = -70°$ and $165 \leq \Psi \leq 175$; and for $\phi = -75°$, $\Psi = +170°$. Outside of this range, the predicted spectra had one or more features that conflict with experiment. The spectra deemed to be in acceptable agreement with experiment have a positive long-wavelength $n\pi^*$ band with $\Delta\varepsilon_{max} < 2\ M^{-1}\ cm^{-1}$; a negative 200-nm band with $||\Delta\varepsilon_{max}|| > 6\ M^{-1}\ cm^{-1}$; and a short-wavelength positive band with $\Delta\varepsilon_{max} < 2\ M^{-1}\ cm^{-1}$. (All calculated CD spectra have a positive band on the short-wavelength edge of the $\pi\pi^*$ region. The experimental CD spectra of P_{II}, as seen in the spectrum of poly(Pro) and in homopolymers that are believed to have a substantial P_{II} content such as poly(Glu) and poly(Lys), remain negative to ~160 nm.[24,25] However, the spectrum of poly(Glu) (Figure 1) has a minimum magnitude near zero at ~178 nm and both poly(Glu) and poly(Pro) show evidence of an additional negative band at shorter wavelengths, probably due to an interamide charge transfer transition, known[51−53] to occur between the NV_1 and NV_2 transitions but not considered in our calculations. Therefore a modest positive band near 180 nm in calculations omitting

(46) Moffitt, W.; Fitts, D. D.; Kirkwood, J. G. *Proc. Natl. Acad. Sci. U.S.A* **1957**, *43*, 723–730.
(47) Tinoco, I., Jr. *J. Am. Chem. Soc.* **1964**, *86*, 297–298.
(48) Woody, R. W. *Monatsh. Chem.* **2005**, *136*, 347–366.
(49) Pysh, E. S. *J. Chem. Phys.* **1970**, *52*, 4723–4733.
(50) In his 1967 paper, Pysh[16] predicted a strong negative helix band for the P_{II} helix in the standard conformation. Thus, he predicted a negative couplet centered near 190 nm that, in combination with the negative contribution from the polarizable groups, gave qualitatively satisfactory agreement with experiment. However, Pysh used the equation for the helix band given by Tinoco[47] that, through a misprint, was lacking a minus sign.[48] If the correct sign for the helix band is used, a positive couplet is predicted for the standard P_{II} conformation, in agreement with the present results. It should also be noted that Pysh obtained a positive couplet in his 1970 paper,[49] which used explicit matrix diagonalization rather than Tinoco's equation.

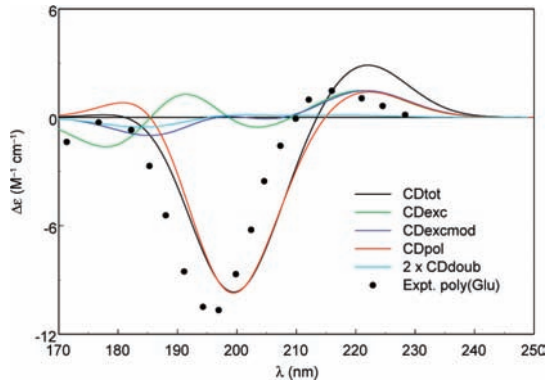

Figure 3. Calculated CD spectrum of $(Ala)_{20}$ with $(\phi, \Psi) = (-60, +160)$. The angle of the 190-nm $\pi\pi^*$ transition moment was taken to be $-40°$. The total CD spectrum is shown in black. The exciton spectrum calculated with exciton wavelengths is shown in green, the exciton spectrum calculated with wavelengths shifted by mixing with high-energy transitions is shown in blue, and the polarizability contribution is in red. The cyan curve is the contribution of mixing with doubly excited configurations, multiplied by a factor of 2 for easier visualization. In this latter calculation, the unmodified exciton wavelengths were used. The experimental CD spectrum of poly(Glu) in water[25] is also shown (black dots).

any transition between the NV_1 and NV_2 transitions is considered to be compatible with experiment.)

Figure 3 shows the CD spectrum calculated for $(Ala)_{20}$ in the $(-60, +160)$ conformation using $\theta = -40°$. The exciton contribution calculated using exciton wavelengths (green curve) has the same pattern of CD bands, with respect to sign, as that for the standard P_{II} conformation with $\theta = -55°$ (Figure 2), but the amplitude of the short-wavelength couplet is reduced by nearly an order of magnitude. The exciton contribution calculated with wavelengths shifted by mixing with high-energy transitions (blue curve) does not show the reversal in sign of the short-wavelength couplet seen with the canonical P_{II} at $\theta = -55°$ (Figure 2), but the positive lobe has nearly vanished and the overall magnitude of the modified exciton contribution remains small. The polarizability contribution (red curve) is strongly nonconservative, with a strong negative band near 200 nm and weak positive maxima in the $n\pi^*$ region and near 180 nm. The resulting total CD spectrum (black curve) is in excellent qualitative agreement with the experimental CD spectrum of poly(Glu) as a model for a P_{II} helix of poly(Ala) (Figure 1). It should be noted that the amplitude of the 200-nm band in Figure 3 is about -10 M^{-1} cm^{-1}. Although this is nearly as large as that of poly(Glu) (Figure 1),[25] poly(Glu) contains less than 100% P_{II} helix at room temperature, perhaps as little as 50%. Thus the true magnitude of poly(Ala) in the P_{II} form may be as much as -20 M^{-1} cm^{-1}. Substantially larger values for the 200-nm CD, approaching -16 M^{-1} cm^{-1}, are predicted for $\phi = -60°$ or $-65°$ and Ψ values near the upper limit investigated ($+185°$).

The cyan curve in Figure 3 shows the contribution of the mixing of the exciton transitions with doubly excited configurations, as described in eq 19. Even after multiplying by a factor of 2 to make it distinguishable from the baseline in the long-wavelength region, this contribution is small. Therefore, its neglect in all previous calculations led to little error. Nevertheless, because inclusion of this effect requires little additional computational effort, it is preferable to include it.

Calculations have also been performed for P_{II} helices of $(Ala)_n$ with $n = 2-20$ and the conformation $(\phi, \Psi) = (-60, +160)$ to assess the helix-length dependence of the CD. The resulting spectra are given in Figure S2 (Supporting Information). The P_{II} CD signature is predicted even for $n = 2$, i.e., with two amide groups. The long-wavelength positive band has nearly the same wavelength and amplitude per amide for all n. The short-wavelength negative band is smaller in amplitude for $n = 2$ than for longer helices and is blue-shifted to 185 nm. There is a small positive shoulder near 200 nm for $n = 2$, which is substantially weaker for $n = 3$ and is absent for $n \geq 4$. As the helix length increases, the short-wavelength negative band increases in magnitude and red shifts to 196 nm. For $n \geq 6$, the only effect of increasing helix length is the enhancement of the negative band.

The helix-length dependence has been analyzed by fitting the two predicted CD maxima to the empirical equation:[54,55]

$$\Delta\varepsilon_\lambda(n) = \Delta\varepsilon_\lambda(\infty)(n - k)/n \tag{29}$$

where n is the number of amides; $\Delta\varepsilon_\lambda(\infty)$ is the CD per amide in an infinite helix; and k is an end-effect correction. This equation can be rearranged to

$$n\Delta\varepsilon_\lambda(n) = \Delta\varepsilon_\lambda(\infty)n - k\Delta\varepsilon_\lambda(\infty) \tag{30}$$

which indicates that a plot of $n\Delta\varepsilon_\lambda(\infty)$ vs n gives a straight line. The CD per amide can be obtained from the slope and k from the intercept. Figures S3 and S4 in the Supporting Information give such plots for the short-wavelength negative band near 195 nm and the positive band near 220 nm. The CD per amide for the 195-nm band is -12.53 M^{-1} cm^{-1} and that for the 220-nm band is 2.72 M^{-1} cm^{-1}. The end-effect corrections for the two bands are 2.7 and -0.7, respectively. The end effect for the 195-nm band shows that the apparent helix length is reduced by about one turn whereas that for the 220-nm band indicates that the apparent helix is about one amide *longer*. The persistence of the P_{II} CD pattern to very short helices is consistent with the observation of this pattern in di- and tripeptides[6] and even in N-acetylamino acids,[56] if one considers the C-terminal carboxylate as a pseudoamide

Figure 4 shows how the polarizable groups modify the total CD for the $(-60, 160)$ conformation. The exciton rotational strengths are represented as blue bars, and the polarizable group contributions as red bars. For clarity, the red bars are shifted by 0.1 nm to longer wavelengths. This figure illustrates the striking result that for each of the exciton levels in the 194−195 nm region, polarized perpendicular to the helix axis, the polarizable group contribution is opposite in sign to the exciton rotational strength. For the four major bands, the polarizable group contribution has a magnitude that is, on average, 77% of the exciton magnitude. By contrast, the polarizability contribution associated with the long-wavelength exciton band, near 197 nm, is of the same sign as the exciton contribution and is nearly equal in magnitude. This is the parallel-polarized exciton band. Thus the polarizable group contributions largely cancel the

(51) Serrano-Andres, L.; Fülscher, M. P. *J. Am. Chem. Soc.* **1998**, *120*, 10912–10920.
(52) Serrano-Andres, L.; Fülscher, M. P. *J. Phys. Chem. B* **2001**, *105*, 9323–9330.
(53) Hirst, J. D.; Colella, K.; Gilbert, A. T. B. *J. Phys, Chem. B* **2003**, *107*, 11813–11819.
(54) Chen, Y. H.; Yang, J. T.; Martinez, H. M. *Biochemistry* **1972**, *11*, 4120–4131.
(55) Gans, P. J.; Lyu, P. C.; Manning, M. C.; Woody, R. W.; Kallenbach, N. R. *Biopolymers* **1991**, *31*, 1605–1614.
(56) Gokce, I.; Woody, R. W.; Anderluh, G.; Lakey, J. H. *J. Am. Chem. Soc.* **2005**, *127*, 9700–9701.

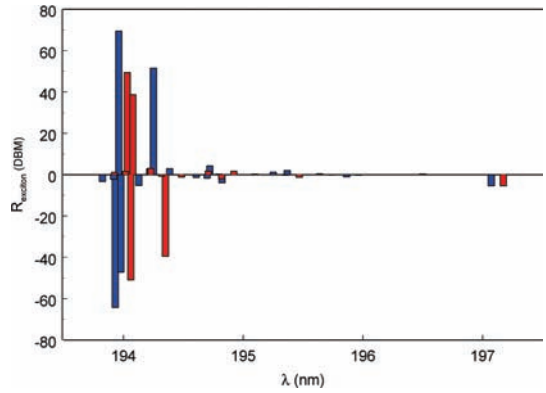

Figure 4. Distribution of exciton rotational strengths for the P_{II} conformation of $(Ala)_{20}$ with $(\phi, \Psi) = (-60, +160)$. The blue bars represent the rotational strengths from the exciton calculation. The red bars represent the polarizability contributions to the exciton levels. The wavelengths for the red bars are offset by 0.1 nm. Note that each exciton band in the short wavelength region is paired with a polarizable group contribution of opposite sign and similar but smaller magnitude. This is not the case for the parallel-polarized exciton band at long wavelengths, for which the two contributions are of the same sign.

Table 2. Contributions[a] of Polarizable Groups to Rotational Strengths of Discrete Transitions for $(Ala)_{20}$ in P_{II} Conformation (−60,160)

group	$R_{n\pi^*}$	R_{NV1}	R_{NV2}
C′═O	−0.0134	−0.0673	0.3014
O lone pair 1	−0.0048	0.0046	0.0838
O lone pair 2	−0.0034	−0.0323	0.1140
$C_\alpha-C'$	−0.0052	−0.0628	0.0976
C′−N	−0.0169	−0.0036	0.1063
N−H	−0.0051	−0.0187	0.0138
$N-C_\alpha$	−0.0080	−0.0103	0.0200
$\pi\pi^*$ trans[b]	−0.0068	−0.0308	−0.0041
$C_\alpha-H$	0.0078	0.0436	−0.0426
$C_\alpha-C_\beta$	0.0301	−0.0076	0.0359
Me_β	0.0731	−0.0053	0.0791
total	0.0475	−0.1905	0.8053

[a] In DBM per residue. [b] The "group" labeled '$\pi\pi^*$ trans' corresponds to the polarizability contributions of the 190- and 140-nm $\pi\pi^*$ transitions.

perpendicularly polarized exciton CD bands and reinforce the parallel-polarized exciton band. These factors, plus the polarizability-induced wavelength shifts, are responsible for replacing the conservative exciton band, with its positive couplet centered at 186 nm, by a strong negative CD band centered near 200 nm, the approximate position of the parallel-polarized exciton band.

The contributions of the various polarizable groups to the rotational strengths of the discrete transitions in the P_{II} (−60, +160) conformation of $(Ala)_{20}$ are shown in Table 2. The total contributions for the nπ^*, NV_1, and NV_2 transitions are, respectively, +0.0475, −0.1905, and 0.8053 DBM. The sizable net negative contribution to the NV_1 transition is responsible for the nonconservative CD band of the P_{II} conformation. For the NV_1 transition, all polarizabble groups, except for one of the oxygen lone pairs and the $C_\alpha-H$ bond, make negative contributions, with those of the C′═O and $C_\alpha-C'$ bonds being largest in magnitude. The $C_\alpha-C_\beta$ and $C_\beta-$methyl groups of the side chain make relatively small contributions to the NV_1 rotational strength in the P_{II} helix. For the nπ^* transition, by contrast, the $C_\alpha-C_\beta$ and $C_\beta-$methyl groups dominate the polarizable group contributions and are almost solely responsible for the positive sign. The polarizable group contributions are

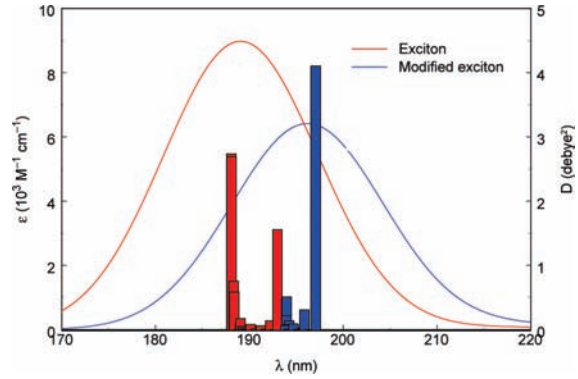

Figure 5. Calculated absorption spectrum (left axis) for $(Ala)_{20}$ in the P_{II} conformation with $(\phi, \Psi) = (-60, +160)$. The red spectrum is the exciton-only spectrum and the blue spectrum includes the effects of mixing with high-energy transitions on the exciton wavelengths and on the dipole strengths. The dipole strengths (right axis) and wavelengths of the exciton bands are represented by red and blue bars. The original exciton intensities and wavelengths are shown by the red bars and the blue bars show the modified exciton bands. Note the decreased intensity of the short-wavelength perpendicular-polarized and the increased intensity of the long-wavelength parallel-polarized band after mixing with high-energy transitions.

largest for the NV_2 transition, in part because of its higher energy. They are almost uniformly positive, with the largest being those of the C′═O, $C_\alpha-C'$, and C′−N bonds and one of the oxygen lone pairs.

Mixing with high-energy transitions is also predicted to have a significant effect on the absorption spectrum. Figure 5 shows the calculated absorption spectra of the P_{II} helix with and without inclusion of the polarizable group contributions. The dipole strengths of the exciton bands are also shown, before and after correction for mixing with high-energy transitions. The parallel and perpendicular exciton bands are predicted to lie at 193 and 188 nm with dipole strengths of 1.56 and 7.43 D^2, respectively. Mixing with high-energy transitions shifts the bands to 197 (||) and 193 (⊥), with dipole strengths of 4.10 (||) and 2.01 (⊥) D^2. Thus, the polarizable-group interactions decrease the exciton splitting by 1 nm, lead to 32% hypochromism, and shift the principal absorption intensity from the perpendicular to the parallel band, leading to a red shift in λ_{max}^{abs} of 7 nm. The relative intensities of the two bands is related to the apparent angle, δ, of the NV_1 transition moment relative to the helix axis:

$$\tan^2 \delta = D_\perp / D_{||} \qquad (22a)$$

where $D_{||}$ and $D_\perp$ are the dipole strengths of the parallel and perpendicular bands, respectively. The angle δ is 65° in the exciton approximation and 35° after the inclusion of polarizable group contributions. Mandel and Holzwarth's[57] resolution of the CD and linear dichroism spectra of poly(Pro)II gave a value of $\delta = 46°$. The total absorption spectrum is predicted to have $\lambda_{max}^{abs} = 196$ nm, 3 nm to the blue of the CD maximum ($\lambda_{max}^{CD} = 199$ nm). Experimentally the absorption spectrum of poly(Glu) is blue-shifted by about 6 nm relative to the CD spectrum ($\lambda_{max}^{abs} \approx 190$ nm, $\lambda_{max}^{CD} \approx 196$ nm).

We now consider the CD spectrum of Pro-containing peptides in the P_{II} conformation. High-resolution structural data are available for oligomers $(ProProGly)_n$, a collagen model that forms triple helices. Figure 6 shows the predicted CD spectrum of $(ProProGly)_{10}$, calculated for the structure determined by

(57) Mandel, R.; Holzwarth, G. *Biopolymers* **1973**, *12*, 655–674.

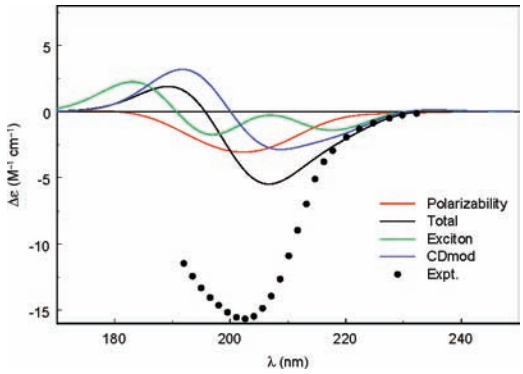

Figure 6. Calculated CD spectrum of $(Pro\text{-}Pro\text{-}Gly)_{10}$, which forms a three-stranded helix that is a model of collagen. The calculations were based on the crystal structure of Kramer et al.[58] (PDB 1A3I) and utilized only 18 residues. The total CD spectrum is shown in black. The exciton spectrum calculated with exciton wavelengths is shown in green, the exciton spectrum calculated with wavelengths shifted by mixing with high-energy transitions is shown in blue, and the polarizability contribution is in red. The experimental spectrum[59] of $(Pro\text{-}Pro\text{-}Gly)_{10}$ is also shown (black dots).

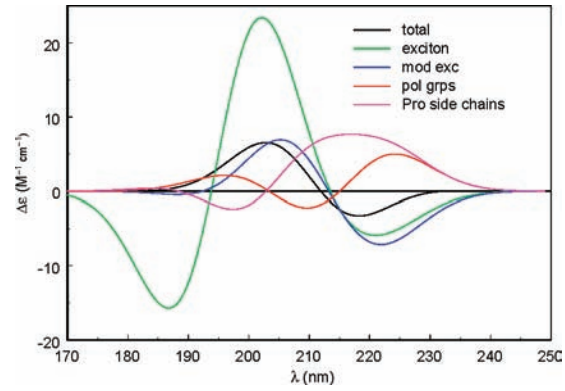

Figure 7. Calculated CD spectrum of $(Pro)_{20}$ in the conformation obtained by Sasisekharan.[62] The total CD spectrum is shown in black. The exciton spectrum calculated with exciton wavelengths is shown in green, the exciton spectrum calculated with wavelengths shifted by mixing with high-energy transitions is shown in blue, and the polarizability contribution is in red. The contribution of the Pro side chains is shown in magenta.

Kramer et al.[58] (PDB 1A3I). The exciton model (green curve) gives a negative couplet centered at 190 nm, a negative band at 218 nm, and a broad, weak, positive band at 234 nm. The polarizability-induced wavelength shifts change the exciton spectrum, enhancing the negative couplet, red-shifting it to ~200 nm, and combining its negative lobe with the negative nπ^* band. The polarizability contributions to the rotational strengths (red curve, Figure 6) give a strong negative band at 202 nm. The total predicted CD (black curve, Figure 6) has a weak, broad, positive band at 237 nm, a negative band at 207 nm, and a positive band at 189 nm. The experimental CD spectrum of poly(ProProGly)[59] (full circles) shows a very weak positive feature above 230 nm and a strong negative band at 205 nm, although the observed magnitude is about 3 times as large ($\Delta\varepsilon_{max} \approx -16\ M^{-1}\ cm^{-1}$) as that calculated here. The data only extend to 190 nm but are still strongly negative at that wavelength. The predicted positive band at 190 nm is not observed.

Two other collagen models have been studied—PDB[60] structures 1A3J[58] and 1K6F.[61] Their predicted spectra differ from that of 1A3I and from each other. The spectrum of 1A3J is predicted to have a negative nπ^* band at 221 nm ($\Delta\varepsilon_{max} = -1.6\ M^{-1}\ cm^{-1}$); a positive NV_1 couplet with a positive band at 209 nm ($\Delta\varepsilon_{max} = 1.0\ M^{-1}\ cm^{-1}$) and a negative band at 196 nm ($\Delta\varepsilon_{max} = -3.0\ M^{-1}\ cm^{-1}$); and a weak positive band at 180 nm ($\Delta\varepsilon_{max} = 0.3\ M^{-1}\ cm^{-1}$). The predicted spectrum of 1K6F has a negative NV_1 couplet, the long-wavelength lobe of which overlaps with a negative nπ^* band to give a negative band at 214 nm with $\Delta\varepsilon_{max} = -6.1\ M^{-1}\ cm^{-1}$ and a positive band at 195 nm ($\Delta\varepsilon_{max} = 2.3\ M^{-1}\ cm^{-1}$). Thus, the calculated CD spectra of these three collagen models, all similar in structure, illustrate the sensitivity of the calculations to the detailed molecular conformation.

Calculations have also been performed for four models of poly(Pro), one based upon the fiber diffraction structure of Sasisekharan[62] and the other three upon the structure of $(Pro)_{10}$[63] (PDB 1AWI) or other Pro-rich peptides[64,65](PDB 2V8C, 1CF0) complexed with profilin. The results for $(Pro)_{20}$ in the Sasisekharan structure are shown in Figure 7. The exciton spectrum (green curve, Figure 7) shows a very strong positive couplet centered at 194 nm and a negative band at 221 nm. The negative lobe of the NV_1 couplet nearly disappears and the positive lobe is diminished and red-shifted upon including wavelength shifts (blue curve, Figure 7). These spectra are similar to those obtained for $(Ala)_{20}$ in the standard P_{II} conformation, apart from a red shift of ~10 nm associated with the lower energy of the NV_1 transition in tertiary amides relative to secondary amides and a difference in sign of the nπ^* band. Mixing with high-energy transitions (red curve, Figure 7) contributes a negative couplet centered at 203 nm and a positive band at 224 nm. Although the polarizable group contributions oppose those from exciton mixing, they are less intense in the 200-nm region, so the exciton effect is dominant. The total predicted CD (black curve, Figure 7) has a positive NV_1 band at 203 nm, a negative nπ^* band at 218 nm, and a very weak positive band at 236 nm.

It is also of interest to consider the contributions of the Pro side chains to the $(Pro)_{20}$ CD spectrum by comparing the spectrum for the Sasisekharan structure calculated with and without the Pro side chains (magenta curve, Figure 7). The Pro side chains are responsible for a positive couplet centered at 203 nm and a positive nπ^* band.

The spectra predicted for $(Pro)_{10}$ and Pro-rich peptides complexed with profilin (PDB 1AWI, 1CF0, 2V8C) are compared with that for the Sasisekharan structure in Figure 8. A positive band is predicted between 200 and 210 nm for all four structures, in contrast to the experimentally observed negative CD band at 206 nm, but the predicted positive CD is more than 5-fold smaller for 1AWI than that of the 1CF0 structure. These intensity differences are not attributable to

(58) Kramer, R. Z.; Vitagliano, L.; Bella, J.; Berisio, R.; Mazzarella, L.; Brodsky, B.; Zagari, A.; Berman, H. M. *J. Mol. Biol.* **1998**, *280*, 623–638.
(59) Bhatnagar, R. S.; Rapaka, R. S. *Biopolymers* **1975**, *14*, 597–603.
(60) Berman, H. M.; Westbrook, J.; Feng, Z.; Gilliland, G.; Bhat, T. N.; Weissig, H.; Shindyalov, I. N.; Bourne, P. E. *Nucleic Acids Res.* **2000**, *28*, 235–242.
(61) Berisio, R.; Vitagliano, L.; Mazzarella, L.; Zagari, A. *Protein Sci.* **2002**, *11*, 262–270.
(62) Sasisekharan, V. *Acta Crystallogr.* **1959**, *12*, 897–903.
(63) Mahoney, N. M.; Janmey, P. A.; Almo, S. C. *Nat. Struct. Biol.* **1997**, *4*, 953–960.
(64) Kursula, P.; Kursula, I.; Massimi, M.; Song, Y. H.; Downer, J.; Stanley, W. A.; Witke, W.; Wilmanns, M. *J. Mol. Biol.* **2008**, *375*, 270–290.
(65) Mahoney, N. M.; Rozwarski, D. A.; Fedorov, E.; Fedorov, A. A.; Almo, S. C. *Nat. Struct. Biol.* **1999**, *6*, 666–671.

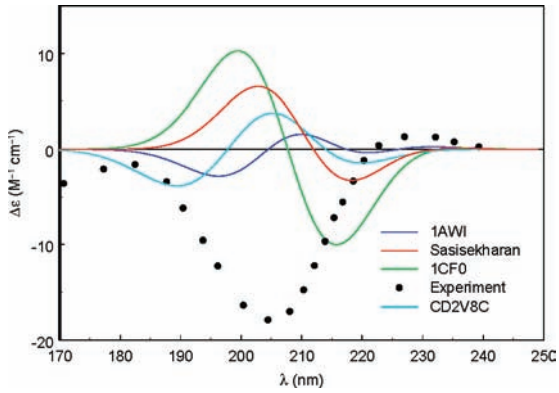

Figure 8. CD spectra for $(Pro)_n$ predicted for four different conformations derived from X-ray diffraction. The red spectrum is that for the Sasisekharan[62] structure from fiber diffraction on poly(Pro). The blue spectrum is for $(Pro)_{10}$ from the crystal structure of a complex with profilin (PDB code 1AWI).[63] The green spectrum is for the oligoPro portion of the peptide Pro_{10}-ITyr (ITyr = 3-iodotyrosine) complexed with profilin (PDB code 1CF0).[65] The cyan spectrum is for the Pro-rich peptide $(GlyPro_5)_3GlyLeu$ complexed with profilin (PDB code 2V8C).[64] The experimental spectrum[2] for poly(Pro) II in water is also shown (black dots).

chain-length effects because the spectrum calculated for a decamer of the Sasisekharan structure has an NV_1 couplet of nearly the same intensity as that of the 20-mer. The differences must be due to conformational differences. The Sasisekharan structure is a uniform helix with all residues having the same (ϕ,Ψ) and the Pro ring with $\chi_1 > 0$, $\chi_2 < 0$, i.e., in the DOWN conformation.[66] By contrast, $(Pro)_{10}$ in 1AWI has ϕ values that alternate between $-60°$ and $-75°$, corresponding to the two classes of Pro residues identified by Ho et al.[67] The Pro ring conformation also varies between UP and DOWN, but not in a regular pattern. In 1CF0, the eight Pro residues have rather uniform ϕ values, ranging from $-65°$ to $-68°$. The χ_1 values also have a narrow range, corresponding to the UP ring pucker. The ten Pro residues of 2 V8C show a large range in ϕ with two outliers at $-59°$ and $-82°$ but, for the rest of the Pro residues, ϕ ranges from $-64°$ to $-69°$. The two Gly residues, one of which is in the middle of the observed peptide, have ϕ values of 180° and $-90°$, adding to the conformational heterogeneity. The ring puckering of the Pro residues in 2V8C is uniformly DOWN. The intensity of the positive band between 200 and 210 nm appears to correlate with the regularity of the helix, being largest for the more regular helices and smallest for the two helices that are more irregular.

Recent studies of oligo- and poly(Pro)[68−72] have shown that in addition to a range of (ϕ,Ψ) angles and ring puckerings, cis isomers must also be considered. Therefore, it appears that poly(Pro) cannot be described as a single, well-defined conformation but must be considered as an ensemble of conformers. It will be necessary to take this into account to obtain a satisfactory description of the CD of poly(Pro), e.g., by coupling CD calculations with MD simulations.

Discussion

This work has important implications for understanding and predicting the CD of proteins and peptides. The inability of the matrix method[41] to correctly calculate the CD spectrum of the P_{II} conformation[4,18,73] has been a serious obstacle to predicting the CD spectrum of proteins. The calculated CD spectra of proteins rich in α-helix and those with significant amounts of both α- and β-structure reproduce the experimental protein spectra reasonably well (for reviews, see refs 74−76). However, for β-rich proteins, the results are less satisfactory. For those β-rich proteins with CD spectra resembling the spectra of model β-sheet polypeptides, called β-I proteins,[77] the CD calculations have shown success comparable to those for α- and αβ-proteins. However, calculations for a second class of β-proteins, called β-II, have been unsuccessful. The experimental CD spectra of these proteins are similar to those of unordered proteins despite the fact that they have a significant amount of β-sheet. Sreerama and Woody[78] showed that the distinction between β-I and β-II proteins lies in the ratio of β-sheet to P_{II} conformation. If this ratio is greater than ~0.4, a β-I spectrum is observed; a ratio less than ~0.4 leads to a P_{II}-like spectrum with a negative band near 200 nm, resembling an unordered-protein CD spectrum. The failure of the standard model for protein CD to reproduce the spectrum of β-II proteins is therefore attributable to the substantial P_{II} content of these proteins. Application of the methods developed in this paper should lead to substantial improvement in the predicted CD spectra of β-II proteins.

The prediction of the CD spectrum of other proteins is also likely to be improved significantly by the methods described here, though less dramatically than in the case of β-II proteins. For many proteins, especially β-I proteins, the CD predicted in the 190−200 nm region is substantially more positive than the observed CD.[34,53,74,75,79,80] It is likely that this is a consequence of the incorrect treatment of the P_{II} component within the unordered conformation, which gives positive CD at these wavelengths, whereas negative CD is observed experimentally. Inclusion of polarizable group effects is expected to improve these results.

Previous efforts to calculate the CD spectrum of unordered polypeptides[42,49,81,82] have been unsuccessful,[4,5] largely because the exciton model gives poor results for the P_{II} conformation. The present results will enable progress in simulating the CD of unordered polypeptides. The conformation of small linear oligopeptides, such as di- and tripeptides, has been a topic of great interest recently. NMR and vibrational spectroscopy have

(66) Nemethy, G.; Gibson, K. D.; Palmer, K. A.; Yoon, C. N.; Paterlini, G.; Zagari, A.; Rumsey, S.; Scheraga, H. A. *J. Phys. Chem.* **1992**, *96*, 6472–6484.
(67) Ho, B. K.; Coutsias, E. A.; Seok, C.; Dill, K. A. *Protein Sci.* **2005**, *14*, 1011–1018.
(68) Doose, S.; Neuweiler, H.; Barsch, H.; Sauer, M. *Proc. Natl. Acad. Sci. U.S.A.* **2007**, *104*, 17400–17405.
(69) Best, R. B.; Merchant, K. A.; Gopich, I. V.; Schuler, B.; Bax, A.; Eaton, W. A. *Proc. Natl. Acad. Sci. U.S.A.* **2007**, *104*, 18964–18969.
(70) Kapitan, J.; Baumruk, V.; Bour, P. *J. Am. Chem. Soc.* **2006**, *128*, 2438–2443.
(71) Schuler, B.; Lipman, E. A.; Steinbach, P. J.; Kumke, M.; Eaton, W. A. *Proc. Natl. Acad. Sci. U.S.A.* **2005**, *102*, 2754–2759.
(72) Watkins, L. P.; Chang, H. Y.; Yang, H. *J. Phys. Chem. A* **2006**, *110*, 5191–5203.
(73) Madison, V.; Schellman, J. *Biopolymers* **1970**, *9*, 569–588.
(74) Sreerama, N.; Woody, R. W. *Methods Enzymol.* **2004**, *383*, 318–351.
(75) Rogers, D. M.; Hirst, J. D. *Chirality* **2004**, *16*, 234–243.
(76) Oakley, M. T.; Bulheller, B. M.; Hirst, J. D. *Chirality* **2006**, *18*, 340–347.
(77) Wu, J.; Yang, J. T.; Wu, C. S. C. *Anal. Biochem.* **1992**, *200*, 359–364.
(78) Sreerama, N.; Woody, R. W. *Protein Sci.* **2003**, *12*, 384–388.
(79) Kurapkat, G.; Krüger, P.; Wollmer, A.; Fleischhauer, J.; Kramer, B.; Zobel, E.; Koslowski, A.; Botterweck, H.; Woody, R. W. *Biopolymers* **1997**, *41*, 267–287.
(80) Bulheller, B. M.; Miles, A. J.; Wallace, B. A.; Hirst, J. D. *J. Phys. Chem. B* **2008**, *112*, 1866–1874.
(81) Aebersold, D.; Pysh, E. S. *J. Chem. Phys.* **1970**, *53*, 2156–2163.
(82) Tonelli, A. E. *Macromolecules* **1969**, *2*, 635–637.

provided important data characterizing the conformational ensemble in small peptides.[8,83−91] The results of these studies, together with data from simulations,[88,92−94] point to a narrower range of conformations than thought previously, and the P_{II} conformation is an important component. In the case of oligo(Ala), the P_{II} conformation is dominant, consistent with CD data. Only a few efforts to calculate the CD spectra of short linear peptides have been reported,[73,95,96] but all of these have been unable to reproduce the experimental CD spectra in water. Strong positive couplets were obtained theoretically, in contrast to the negative CD observed near 200 nm. The methods developed in this paper are likely to yield improved results in the simulation of linear peptide CD spectra.

What effect do the polarizability contributions have on the calculated CD of the α-helix? As noted before, the CD spectrum of the α-helix is nearly conservative, so it is expected that mixing with high-energy transitions will not lead to any significant *net* rotational strength in the NV_1-nπ^* region. However, mixing with high-energy transitions can affect the shape of the α-helix CD spectrum. In fact, calculations for the α-helix (to be published) show that mixing with the high-energy transitions contributes a strong negative couplet centered near $\lambda_\perp$ (∼190 nm) for $\theta_{NV1} = -40°$. Inclusion of the polarizable group contributions improves agreement with experiment relative to the exciton contribution alone. The long-wavelength negative lobe of the couplet from polarizable groups enhances the parallel-polarized negative band near 205 nm. The short-wavelength positive lobe largely cancels the negative lobe of the helix band from the exciton model. The failure to observe the negative lobe of the helix band predicted by exciton theory on the short wavelength side of the $\pi\pi^*$ band[25,97] has long been recognized as a weakness of the theory. The effects of the high-energy transitions rectify this difficulty.

It should be noted that for $\theta_{NV1} = -55°$, the polarizable group contribution gives a *positive* couplet centered near 190 nm. In this case, the polarizable group contribution diminishes the negative band near 205 nm and enhances the short-wavelength negative band, thus leading to poorer agreement with experiment. Therefore, the results for both the P_{II}- and α-helix, when polarizabilities are included, are improved by the use of $\theta_{NV1} = -40°$ and worsened by $\theta_{NV1} = -55°$. Using $\theta_{NV1} = -55°$ in exciton-only calculations, rather than $\theta_{NV1} = -40°$, simulates in part the inclusion of polarizable group contributions in calculations on the α-helix and perhaps on the β-sheet, but not on P_{II} helices.

Three earlier studies of other systems have utilized approaches that are similar in many respects to the one used in this work. Johnson and Tinoco[98] developed a formalism for calculating the contributions of high-energy transitions to the exciton states derived from discrete low-energy transitions. They summed over the exciton levels and calculated the polarizable group contributions to the exciton CD spectrum as a Taylor's series expansion, retaining only the first two terms. The first term of the series gives the net contribution of the high-energy transitions and has the band shape of the discrete transition(s). The second term takes into account the variation of the high-energy contribution with the exciton levels and has a band shape like that of the derivative of the band-shape function for the discrete transition(s), i.e., it is a couplet. Johnson and Tinoco's theory was developed for applications to nucleic acids, and it is useful for treating the electrically allowed $\pi\pi^*$ transitions of the bases in the 240−280 nm region. Because it uses an expansion about a specific wavelength, the range of the transitions included must be relatively small. The theory's applicability to polypeptides is limited by the restricted wavelength range, plus the need to consider the mixing of the $\pi\pi^*$ transitions with the electrically forbidden nπ^* transition.

Zubkov and Vol'kenshtein[28] used an extended version of the exciton model for calculating rotational strengths that is essentially identical to that used here, except that the contributions of magnetically allowed transitions and wavelength shifts were neglected. In addition, the older unreliable polarizability parameters[22] were used. Zubkov and Vol'kenshtein considered the α-helix and β-sheet, but not the P_{II}-helix. Their polarizability calculations for the α-helix predicted a positive couplet centered at $\lambda_\perp$, which would exacerbate the problem of the unobserved negative lobe of the exciton helix band. This difficulty was masked in their paper because they also included the effects of mixing the NV_1 transition with the n$'\pi^*$ and nσ^* amide transitions, which gave a somewhat larger negative couplet. These two transitions, falling between the NV_1 and NV_2 transitions, were tentatively assigned from gas-phase amide spectra[99] and were used in some of the early calculations of polypeptide CD spectra.[16,22] Crystal spectra of amides do not show these transitions in this wavelength region,[36] so they should be neglected.

Rabenold and Rhodes[30] used a time-dependent Hartree formalism. For polarizabilities, they used three different tensors, two based upon Applequist's work[100] and one upon Ronish and Krimm's.[19] The three models gave qualitatively similar results. The results of Rabenold and Rhodes agree with our results for the α-helix, the only system to which they applied their model, in that they predict that the polarizable groups give rise to a

(83) Schweitzer-Stenner, R. *Biophys. J.* **2002**, *83*, 523–532.
(84) Schweitzer-Stenner, R.; Eker, F.; Griebenow, K.; Cao, X. L.; Nafie, L. A. *J. Am. Chem. Soc.* **2004**, *126*, 2768–2776.
(85) Eker, F.; Griebenow, K.; Cao, X. L.; Nafie, L. A.; Schweitzer-Stenner, R. *Proc. Natl. Acad. Sci. U.S.A.* **2004**, *101*, 10054–10059.
(86) Eker, F.; Griebenow, K.; Cao, X. L.; Nafie, L. A.; Schweitzer-Stennert, R. *Biochemistry* **2004**, *43*, 613–621.
(87) Eker, F.; Griebenow, K.; Schweitzer-Stenner, R. *J. Am. Chem. Soc.* **2003**, *125*, 8178–8185.
(88) Graf, J.; Nguyen, P. H.; Stock, G.; Schwalbe, H. *J. Am. Chem. Soc.* **2007**, *129*, 1179–1189.
(89) Grdadolnik, J.; Grdadolnik, S. G.; Avbelj, F. *J. Phys. Chem. B* **2008**, *112*, 2712–2718.
(90) Hagarman, A.; Measey, T.; Doddasomayajula, R. S.; Dragomir, I.; Eker, F.; Griebenow, K.; Schweitzer-Stenner, R. *J. Phys. Chem. B* **2006**, *110*, 6979–6986.
(91) McColl, I. H.; Blanch, E. W.; Hecht, L.; Kallenbach, N. R.; Barron, L. D. *J. Am. Chem. Soc.* **2004**, *126*, 5076–5077.
(92) Garcia, A. E. *Polymer* **2004**, *45*, 669–676.
(93) Kentsis, A.; Mezei, M.; Osman, R. *Proteins-Struct. Funct. Bioinform.* **2005**, *61*, 769–776.
(94) Zagrovic, B.; Lipfert, J.; Sorin, E. J.; Millett, I. S.; van Gunsteren, W. F.; Doniach, S.; Pande, V. S. *Proc. Natl. Acad. Sci. U.S.A.* **2005**, *102*, 11698–11703.
(95) Dungan, J. M.; Hooker, T. M. *Macromolecules* **1981**, *14*, 1812–1822.
(96) Rae, I. D.; Leach, S. J.; Minasian, E.; Smith, J. A.; Zimmerman, S. S.; Weigold, J. A.; Hodes, Z. I.; Nemethy, G.; Woody, R. W.; Scheraga, H. A. *Intl. J. Pept. Protein Res.* **1981**, *17*, 575–592.
(97) Cassim, J. Y.; Yang, J. T. *Biopolymers* **1970**, *9*, 1475–1502.
(98) Johnson, W. C., Jr.; Tinoco, I., Jr. *Biopolymers* **1969**, *7*, 727–749.
(99) Barnes, E. E.; Simpson, W. T. *J. Chem. Phys.* **1963**, *39*, 670–675.
(100) Applequist, J. *J. Chem. Phys.* **1979**, *71*, 4332–4338.

negative couplet centered near $\lambda_{\perp}$, largely canceling the short-wavelength negative lobe of the exciton helix band.

Conclusions

By including mixing of the amide $\pi\pi^*$ transition with high-energy transitions modeled by polarizabilities, the strong negative CD of P_{II} peptides can be explained. Although the calculated CD spectrum for the canonical P_{II} structure does not agree with experiment, structures in the P_{II} region with less negative ϕ and more positive Ψ than the canonical values give predicted spectra in agreement with experimental CD spectra for poly(Glu) and poly(Lys), polypeptides known to have substantial P_{II} content. Calculations for some model collagen structures also show agreement with experiment. Calculations for poly(Pro) itself do not give good agreement with experiment, probably because of irregularities in the actual structure associated with variations in (ϕ,Ψ), ring puckering, and cis/trans isomerism.

Acknowledgment. I thank Dr. Walter Stevens for providing the bond and lone-pair polarizability tensors for *N*-methylacetamide used in this work. Early stages of this study were supported by NIH Grant No. EB002803.

Supporting Information Available: Equations 6, 14, and 19−21 in the text are derived; Tables S1−S4 provide details of the polarizability parameters; Tables S5−S8 detail the parameters for the amide nπ^*, NV_1, and NV_2 transitions, including corrections to those used by Woody and Sreerama;[34] Figure S1 compares the exciton CD calculated for an $(Ala)_{20}$ α-helix using the Woody and Sreerama parameters and the corrected parameters used here; Figures S2−S4 show the length-dependence of the CD for the P_{II} helix of $(Ala)_n$. This material is available free of charge via the Internet at http://pubs.acs.org.

JA901218M